

The Effects of Rotation Rate on Deep Convection in Giant Planets with Small Solid Cores

Martha Evonuk* and Gary A. Glatzmaier

Department of Earth Sciences, University of California, 1156 High St., Santa Cruz, CA

95064 USA

*Corresponding author. E-mail: mevonuk@es.ucsc.edu, Fax: 831-459-3074

Now at: Institut fuer Geophysik, ETH Zuerich, Switzerland

Abstract

10 We study how the pattern of thermal convection and differential rotation in the
11 interior of a giant gaseous planet is affected by the presence of a small solid core as a
12 function of the planetary rotation rate. We show, using 2D anelastic, hydrodynamic
13 simulations, that the presence of a small solid core results in significantly different flow
14 structure relative to that of a fully convective interior only if there is little or no planetary
15 rotation.

16 *Keywords:* Planets; Rotation; Jupiter; Internal Convection; Stellar Interiors

1. Introduction

20 Rotation significantly affects the internal structure and dynamics of giant gaseous
21 bodies such as giant planets and stars. The vorticity generated by fluid rising or sinking
22 through the density-stratified interior of a planet or a star and the resulting nonlinear
23 convergence of angular momentum flux maintains differential rotation in the interior and

24 zonal winds at the surface (Evonuk and Glatzmaier, 2006; Glatzmaier et al., in
25 preparation). The strength and pattern of the resulting shear flow depends on the rotation
26 rate and the rate of internal heating, that is, the strength and nature of convection.

27 A related feature of interest concerns the presence of small solid or otherwise
28 non-interacting cores in these bodies. In particular, does the fluid behavior change
29 significantly with the presence of a small non-convecting core? This question is of
30 interest for two reasons. First, it is likely that a significant percentage of extra-solar
31 gaseous planets have fully convective interiors. Giant planets are believed to have
32 formed either through accretion of a solid core followed by the capture of surrounding
33 gaseous hydrogen and helium (Pollack et al., 1996) or possibly by direct gravitational
34 instability of the gas in the disk (Boss, 1998). After the giant planets form their cores
35 may erode. Core erosion can occur if the heavy elements are at least partially soluble in
36 the hydrogen helium envelope and if there is sufficient convective energy to overcome
37 the molecular weight barrier that is created (Stevenson, 1982). However, initially high
38 central temperatures (\sim 30,000K) favor solubility of the heavy elements (Guillot, 2005)
39 and could allow significant core erosion via convection or tidal interactions and
40 subsequently result in fully convective planets (Guillot et al., 1994). In our own solar
41 system, one-dimensional structure models of Jupiter indicate that its core must be less
42 than 10 Earth masses; it has no core in extreme models that assume a particular hydrogen
43 EOS, a large J_4 value and an enhancement in heavy elements by 4 to 6 times the solar
44 value (Guillot, 1999). A second reason to study the behavioral differences between fluid
45 bodies with and without non-convecting cores is that most three-dimensional, global,
46 hydrodynamic models of stars and giant gaseous planets, because of the numerical

47 methods, are not able to simulate convection without a solid core (e.g., Glatzmaier, 1984;
48 Sun et al., 1993; Aurnou and Olson, 2001; Christensen, 2001; Brun et al., 2003; Kuhlen
49 et al., 2005). Consequently it is important to know if the presence of a non-convecting
50 core causes a significant change in the fluid flow patterns, relative to a fully convective
51 planet, at various rotation rates.

52 We compare via 2D numerical simulations fluid behavior in giant planets with
53 rapid rotation (period of 10 hours), with slow rotation (2 months), and in the extreme case
54 with no rotation for identical size, mass, and heating rates. We show that at high rotation
55 rates the case with a small core is essentially equivalent to that with no core; and
56 conclude that models that are unable to remove the solid core produce solutions that are
57 reasonable approximations for cases without a core. However at low rotation rates, the
58 geometry of the simulation becomes more important. The fluid in a body with no core
59 develops a dipolar flow structure. This differs significantly from the multi-cell structure
60 formed in a body with a small core. Therefore, models that include a solid, non-
61 convecting core are inappropriate for studying slowly rotating fully convective bodies,
62 such as tidally locked planets in orbits close to their host star or fully convective A-type
63 stars.

64

65 **2. The Numerical Method**

66 The test cases are two-dimensional (2D) time-dependent nonlinear computer
67 simulations of thermal convection in the equatorial plane of a planet with central gravity.
68 We chose to model the planets in two dimensions to provide higher resolution and obtain

69 more turbulent flow. Of course this advantage is offset by the fact that 2D simulations
 70 can not capture all the internal dynamics of a 3D fluid sphere.

71 The following anelastic equations of momentum (1), heat (2), and mass
 72 conservation (3) are solved with the finite volume method on a Cartesian grid as in
 73 Evonuk and Glatzmaier (2006):

$$74 \quad \frac{\partial}{\partial t}(\bar{\rho}u) = -\nabla \cdot \left[\bar{\rho}u_i u_j - P\delta_{ij} - 2\nu\bar{\rho} \left(e_{ij} - \frac{1}{3}\nabla \cdot u\delta_{ij} \right) \right] - \rho\bar{g}\hat{r} + 2\bar{\rho}u \times \Omega - \rho\Omega \times (\Omega \times r), \quad (1)$$

$$75 \quad \frac{\partial}{\partial t}(\bar{\rho}S) = -\nabla \cdot \left[\bar{\rho}(S + \bar{S})u - \kappa_t \bar{\rho} \nabla S - \frac{C_p \kappa_r \bar{\rho}}{\bar{T}} \nabla T \right] + \frac{\bar{\rho}}{\bar{T}} \frac{dT}{dr} \left[\kappa_t \frac{\partial S}{\partial r} + \frac{C_p \kappa_r}{\bar{T}} \frac{\partial T}{\partial r} \right] + \bar{\rho}Q_s, \quad (2)$$

$$76 \quad \text{and } \nabla \cdot (\bar{\rho}u) = 0, \quad (3)$$

77 where ρ is the density, u is the velocity vector, P is the pressure, ν is the turbulent viscous
 78 diffusivity, $e_{ij} = \frac{1}{2} \left[\frac{\partial u_i}{\partial x_j} + \frac{\partial u_j}{\partial x_i} \right]$ is the rate of strain tensor, g is the gravity, Ω is the rotation
 79 vector, S is the entropy, κ_t is the turbulent diffusivity, C_p is the specific heat capacity at
 80 constant pressure, T is the temperature, κ_r is the radiative diffusivity, and Q_s is the heating
 81 function. The over-barred quantities are prescribed reference state variables that are
 82 functions of only radius, and the viscous and thermal diffusivities are constant.

83 Our model is a simple density-stratified fluid spanning four density scale heights,
 84 which places our outer boundary at 8.9 kilobars if we were modeling Jupiter (Guillot,
 85 1999). It is important to include this density variation not only because density-stratified
 86 fluids behave differently than constant-density fluids (Evonuk and Glatzmaier, 2004), but
 87 also because density-stratification is needed in 2D for the Coriolis force to influence the
 88 fluid flow (Glatzmaier et al., in preparation). We set the turbulent Prandtl number (ν/κ_t)
 89 in the convective zone to 0.1 and the traditional Rayleigh numbers for these cases to a

90 few times 10^{12} . The spatial resolution is 1000x1000 in Cartesian coordinates. **While the**
91 **finite-volume method in this coordinate system eliminates the singularity at the**
92 **center of the disk and allows for nearest neighbor communication (and therefore**
93 **efficient parallelization), it is also much more diffusive than the spectral methods**
94 **usually used and therefore requires more grid points than spectral modes to obtain**
95 **comparable accuracy. High resolution also improves the “roundness” of the**
96 **boundaries and allows the resolution of smaller scale features embedded in the**
97 **larger scale flows.** Each case was run for more than 500,000 numerical time-steps
98 corresponding to 0.002 viscous diffusion times or approximately 200 convective turnover
99 times.

100 The non-convecting cores extend to 10% of the total radius (r_t). The outer 10% of
101 the disks are stable radiative layers providing a buffer between the outer impermeable
102 boundary and the internal convecting fluid. The inner 35% of the disks are heated to
103 drive convection (Evonuk and Glatzmaier, 2006). **The radial heating profile is a fairly**
104 **arbitrary choice and mainly meant to maintain convection. Stars of course are**
105 **heated in their central cores and fluid planets can generate heat from gravitational**
106 **contraction, which is proportional to pressure. However, this latter effect may not**
107 **be significant in planets with electron degeneracy.** The fast rotator spins at about
108 Jupiter’s rotation period of 10 hours, whereas the slow rotator has a two-month period.

109 The Ekman number, the ratio of the viscous forces to the Coriolis force, $Ek = \frac{\nu}{2\Omega D^2}$, is
110 3.0×10^{-8} for the high rotation cases and 4.4×10^{-6} for the low rotation cases.

111

112 **3. Results and Discussion**

113 At higher rotation rates it is difficult to distinguish between the cases with small
114 and no core. Figure 1a and 1b show snapshots of the entropy perturbation overlaid with
115 velocity arrows as viewed from the north with the rotation vector out of the page. The
116 fluid flow is clearly differentiated into prograde motion in the outer part of the disk and
117 retrograde motion in the inner part for both cases, as can also be seen in the plot of the
118 zonal flow with radius (Figure 1c). This differential rotation is maintained by the
119 generation of vorticity as fluid flows through the density stratification. The Coriolis force
120 generates negative vorticity as hot material expands as it rises from the interior of the
121 disk. Likewise sinking material generates positive vorticity in the outer regions of the
122 disk. **One needs to distinguish between the local nonaxisymmetric vorticity**
123 **generation by rising and sinking plumes and the global axisymmetric zonal flow,**
124 **which is maintained by the convergence of the nonlinear product of**
125 **nonaxisymmetric radial flow and nonaxisymmetric longitudinal flow. Part of this**
126 **nonlinear product has an axisymmetric eastward (i.e., prograde) component, which**
127 **accumulates in the outer part of the convection zone, and an axisymmetric**
128 **westward (retrograde) component, which accumulates in the inner part of the**
129 **convection zone. This occurs because plumes sinking from near the surface curve**
130 **westward (i.e., transport westward momentum away from the outer region).** We
131 **focus on sinking plumes near the surface because this mechanism is most effective**
132 **where the density scale height is smallest and the radial velocity is the greatest.** The
133 resulting fluid trajectories cause a nonlinear convergence of prograde momentum in the
134 outer part and retrograde momentum in the inner part (Glatzmaier et al., in preparation).
135 The suppression of large-scale convection shifts the peak kinetic energy to higher wave

136 numbers, as oscillations, instead of traditional convection cells, develop to transport the
137 thermal energy vertically (Figure 1d). These small-scale features, as well as the effect of
138 a larger non-convecting core, are discussed in more detail in Evonuk and Glatzmaier
139 (2006).

140 Removing rotation from the simulations eliminates the effect of the Coriolis force
141 while retaining the effect of the density stratification on convection. Now we see
142 distinctly different flow patterns for the cases with and without solid cores (Figure 2a,b).
143 The case without a solid core forms two nearly symmetric cells with peak flow velocities
144 in the center of the disk which is the most efficient flow pattern for removing the heat
145 generated in the central region. The symmetry of these two cells results in mean zonal
146 flows close to zero through out the disk (Figure 2c). The peak kinetic energy is at wave
147 number one reflecting the dipolar flow structure (Figure 2d). The pattern of convection
148 we see is similar to the lowest symmetric mode ($l = 1, m = 0$) of disturbance analytically
149 predicted by Chandrasekhar (1961) in a fluid sphere. Conversely, in the case with a
150 small core, the core breaks up the flow through the center into smaller cells (Figure 2b).
151 This produces higher kinetic energies throughout the energy spectrum for all but wave
152 number one (Figure 2d). The mean zonal flow in this non-rotating case should average to
153 zero over long times. The prograde zonal flow near the core in Figure 2c is due to the
154 persistence of a dominant cell (Figure 2b) during the time over which this average was
155 made. We expect that in a longer simulation that large cell would eventually dissipate
156 and another would form with the opposite vorticity.

157 In the intermediate case with slow rotation we see convective cell patterns similar
158 to the case with no rotation (Figure 3a,b). However, the non-zero Coriolis forces now

159 organize the flow to maintain a weak differential rotation, prograde in the outer part and
160 retrograde in the inner part, as in the high rotation case (Figure 3c). Although the two
161 cases behave differently at depth they have similar zonal velocities at the base of the
162 radiative zone. This suggests that surface observations of the zonal wind velocities
163 would be indistinguishable. However, magnetic fields generated in the deep interior may
164 have different structures at the surfaces of slowly rotating giant planets with and without
165 small solid cores.

166

167 **4. Summary**

168 This series of simulations illustrate the increasing dominance of the Coriolis
169 effect as the rotation rate increases at a given heating rate, suppressing convection and
170 establishing differential flow in the planet. At high rotation rates, $Ek < 10^{-8}$ for our 2D
171 simulations, the presence of a small non-convecting core has little effect on the structure
172 of the flow. However, in more slowly rotating planets ($Ek > 10^{-5}$ in 2D), the presence of a
173 non-convecting core impedes the tendency for dipolar flow through the center, a
174 potentially important effect in giant planets and stars with slow rotation rates especially
175 in light of possible magnetic field generation and interactions in these bodies. **Similar to**
176 **the 2D results, preliminary low resolution 3D finite-volume anelastic simulations**
177 **without a core show dipolar flow in cases with low rotation rate while cases with**
178 **higher rotation rates have essentially no flow through the center as the fluid**
179 **circulates about the origin instead of flowing through it.**

180

181 **Acknowledgements**

182 Support provided by NASA Planetary Atmospheres Program (NAG5-11220),
183 NASA Outer Planets Program (OPR04-0017-0109), and the Institute of Geophysics and
184 Planetary Physics at the Los Alamos National laboratory and the University of California,
185 Santa Cruz. Computing resources were provided by an NSF MRI funded Beowulf cluster
186 at UCSC and allocations at the Pittsburgh Supercomputing Center, National Center for
187 Atmospheric Research, San Diego Super Computing Center, and NASA Ames.

188

189 References

190 Aurnou, J.M., Olson, P.L., 2001. Strong zonal winds from thermal convection in a
191 rotating spherical shell. *Geophys. Res. Lett.* 28, 2557-2559.

192 Boss, A. P., 1998. Evolution of the solar nebula. IV. Giant gaseous protoplanet
193 formation. *ApJ* 503, 923-937.

194 Brun, A.S., Browning, M., Toomre, J., 2003. Looking deep within an A-type star: Core
195 convection under the influence of rotation. In: Maeder, A., Eenens, P. (Eds.), *Stellar*
196 *Rotation*. *Proceedings IAU Symposium No. 215*.

197 Chandrasekhar, S., *Hydrodynamic and Hydromagnetic Stability*, Oxford University Press,
198 1961.

199 Christensen, U.R., 2001. Zonal flow driven by deep convection in the major planets.
200 *Geophys. Res. Lett.* 28, 2553.

201 Evonuk, M., Glatzmaier, G.A., 2004. 2D studies of various approximations used for
202 modeling convection in giant planets. *Geophys. Astrophys. Fluid Dyn.* 98, 241-255.

203 Evonuk, M., Glatzmaier, G. A., 2006. A 2D study of the effects of the size of a solid
204 core on the equatorial flow in giant planets. *Icarus* 181, 458-464.

205 Glatzmaier, G. A., Evonuk, M., Rogers, T. M. Differential rotation in giant planets
206 maintained by density-stratified turbulent convection. In preparation.

207 Guillot, T., 1999. Interiors of giant planets inside and outside the solar system. *Science*
208 286, 72-77.

209 Guillot, T., 2005. The interiors of giant planets models and outstanding questions. *Ann.*
210 *Rev. Earth & Plan. Sciences.*

211 Guillot, T., Gautier, D., Chabrier, G., Mosser, B., 1994. Are the giant planets fully
212 convective? *Icarus* 112, 337-353.

213 Pollack, J. B., Hubickyj, O., Bodenheimer, P., Lissauer, J. J., Podolak, M., Greenzweig,
214 Y., 1996. Formation of the giant planets by concurrent accretion of solids and gas.
215 *Icarus* 124, 62-85.

216 Kuhlen, M., Woosley, S.E., Glatzmaier, G.A., 2005. Carbon Ignition in Type Ia
217 Supernovae: II. Three-Dimensional Numerical Model. Submitted to *ApJ*.

218 Stevenson, D. J., 1982. Interiors of the giant planets. *Ann. Rev. Earth Planet. Sci.* 10,
219 257-295.

220 Sun, Z.-P., Schubert, G., Glatzmaier, G.A., 1993. Banded surface flow maintained by
221 convection in a model of the rapidly rotating giant planets, *Science* 260, 661.

222

223 **Figure Captions**

224

225 Figure 1: Snapshots at high rotation rate (ten-hour period) of the entropy perturbation
226 overlaid with velocity arrows for the case without a solid core (a) and the case with a
227 solid core (b). High entropy is indicated with lighter shades of red and low entropy with

228 darker shades and the rotation axis is directed out of the page. The velocity arrows are
229 scaled the same for the two cases and for those in the next two figures. Also shown are
230 time averaged plots of the mean zonal wind speed as a function of radius (c) and the
231 kinetic energy spectra as a function of longitudinal wave number (d). The case with no
232 core is shown in these plots with a dashed line.

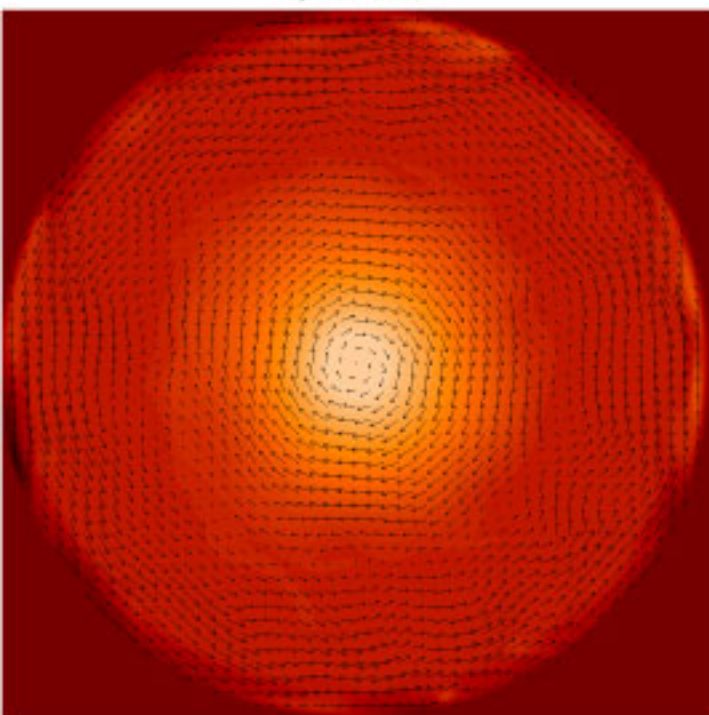
233

234 Figure 2: Same as Figure 1 but for cases with no rotation.

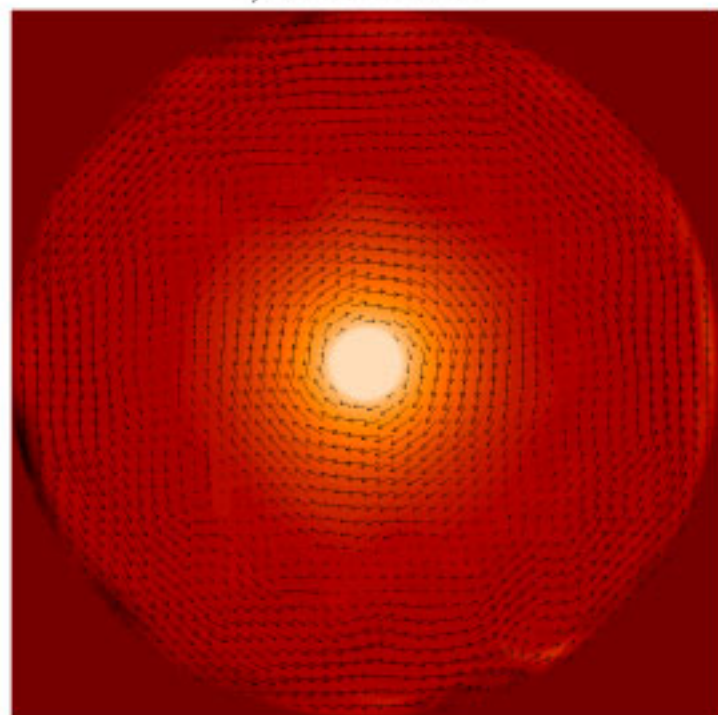
235

236 Figure 3: Same as Figure 1 but for cases with slow rotation rate (two-month period).

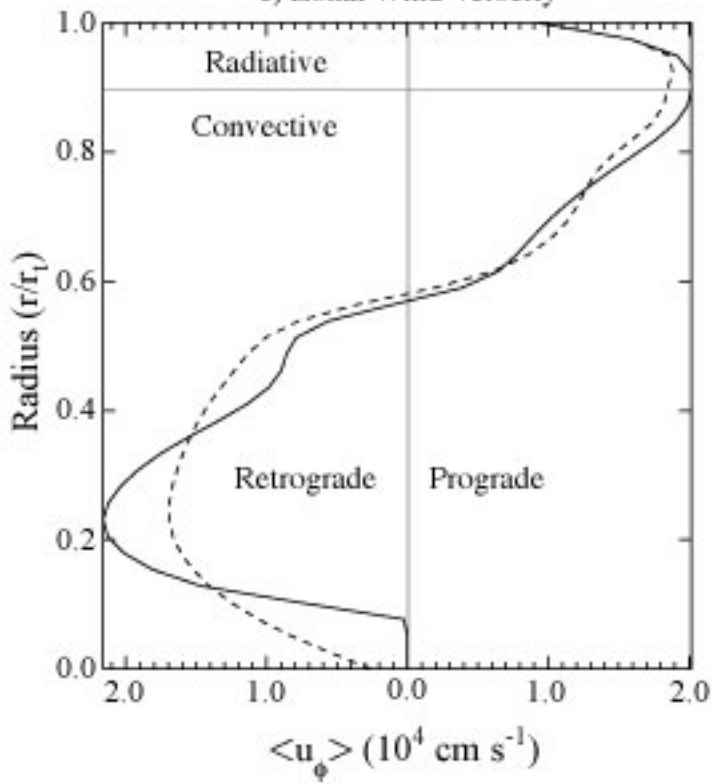
a) No Core



b) Small Solid Core



c) Zonal Wind Velocity



d) Kinetic Energy Spectra

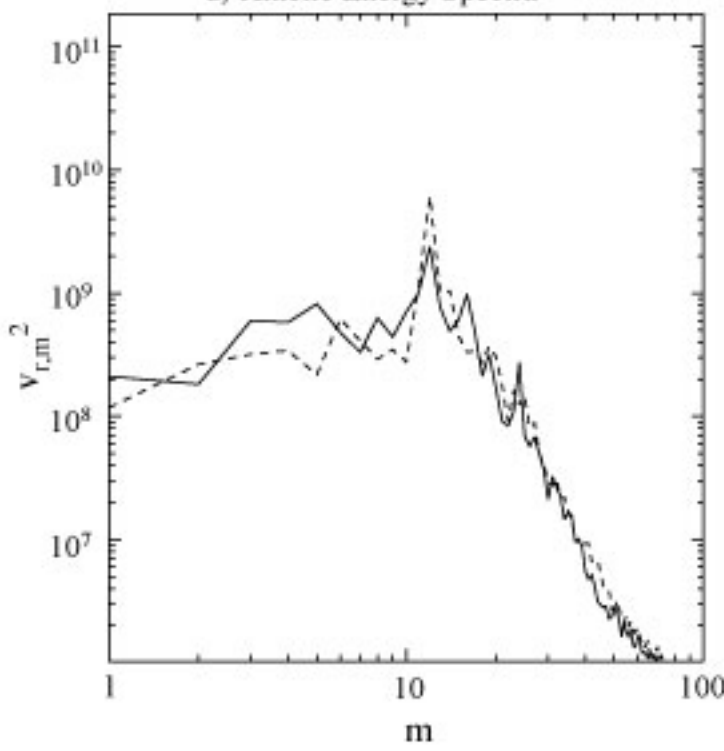
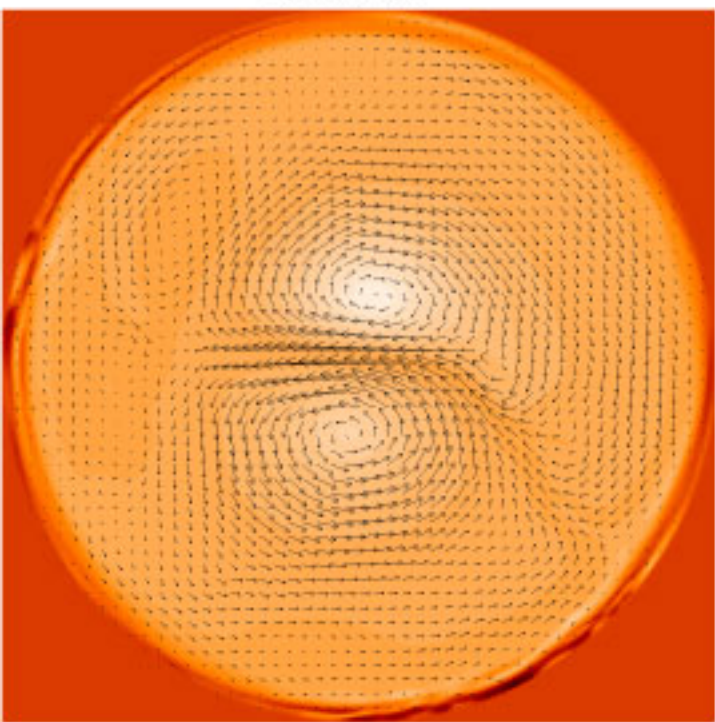
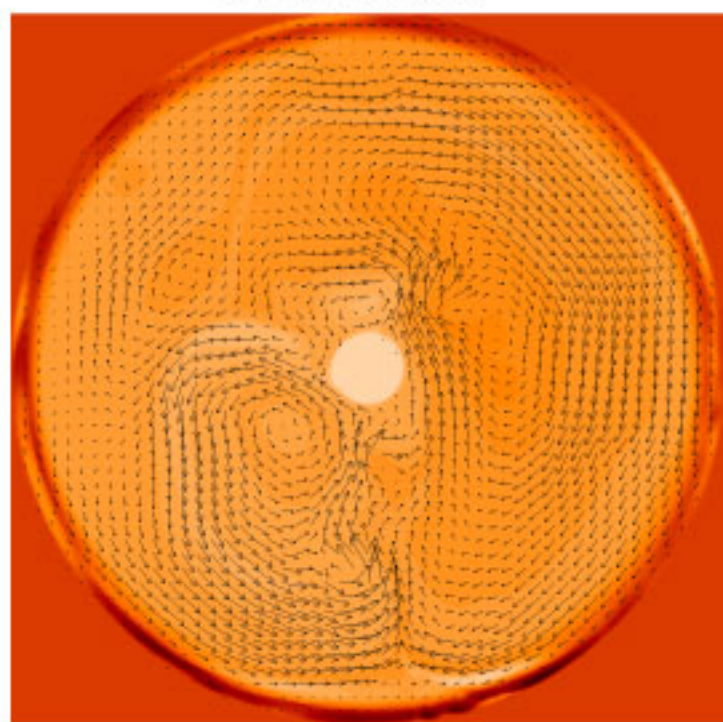


Figure 1: High Rotation Rate

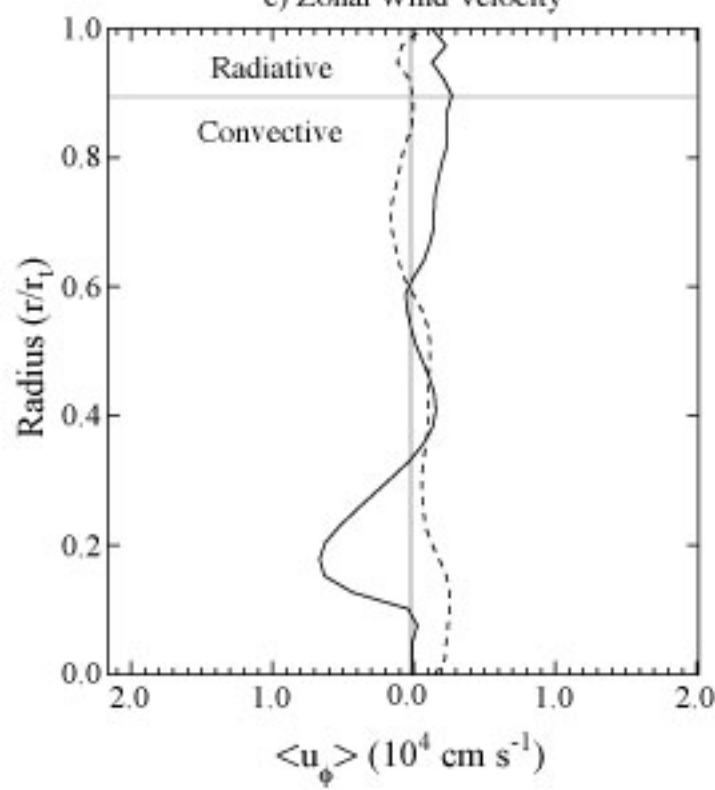
a) No Core



b) Small Solid Core



c) Zonal Wind Velocity



d) Kinetic Energy Spectra

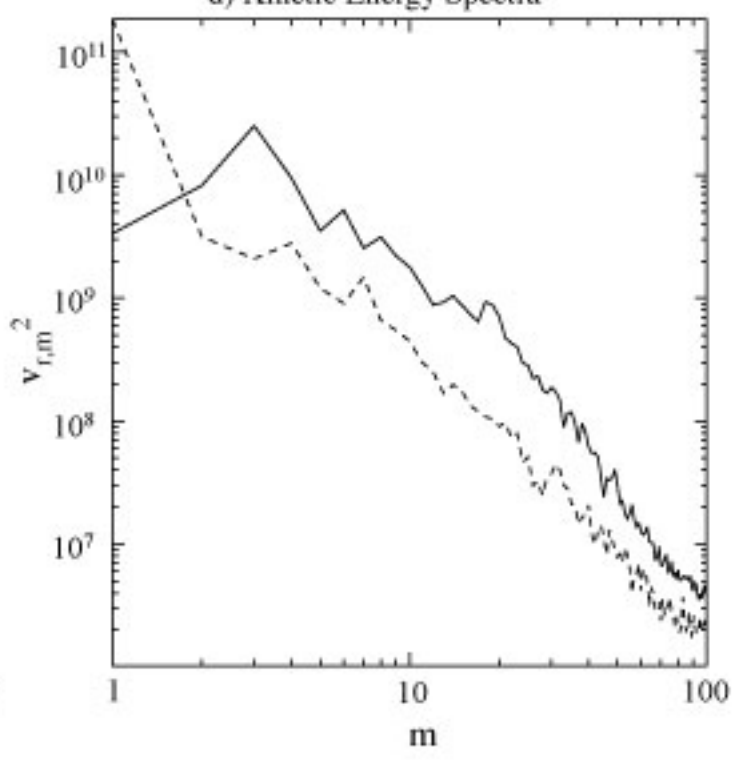
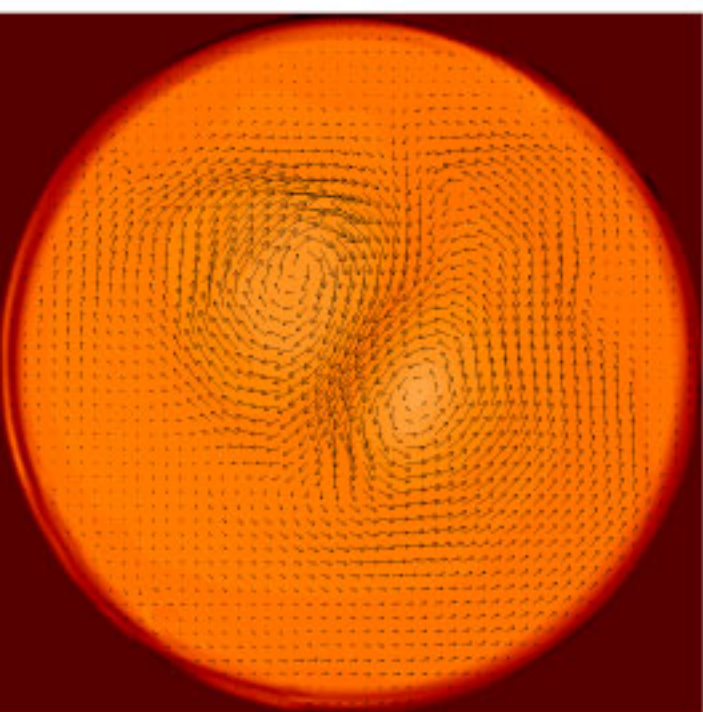
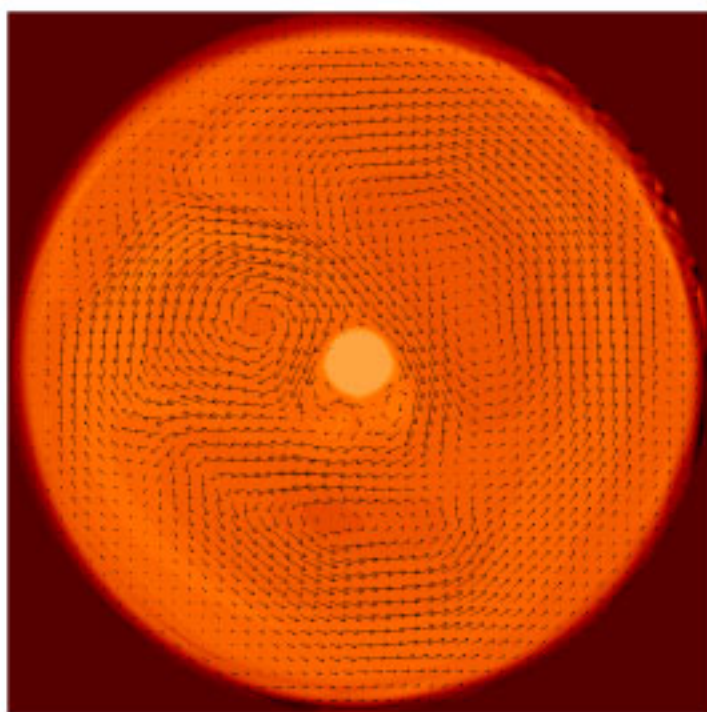


Figure 2: No Rotation

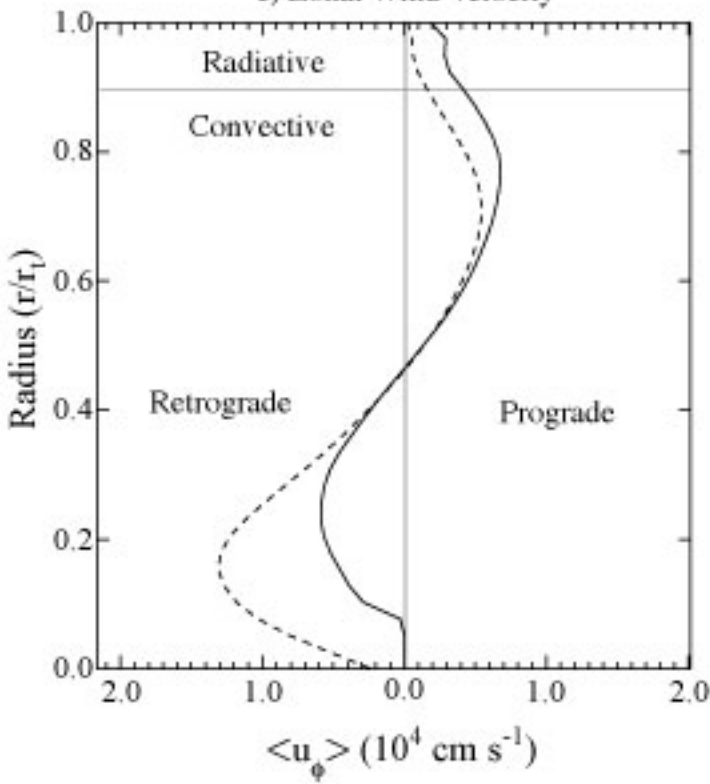
a) No Core



b) Small Solid Core



c) Zonal Wind Velocity



d) Kinetic Energy Spectra

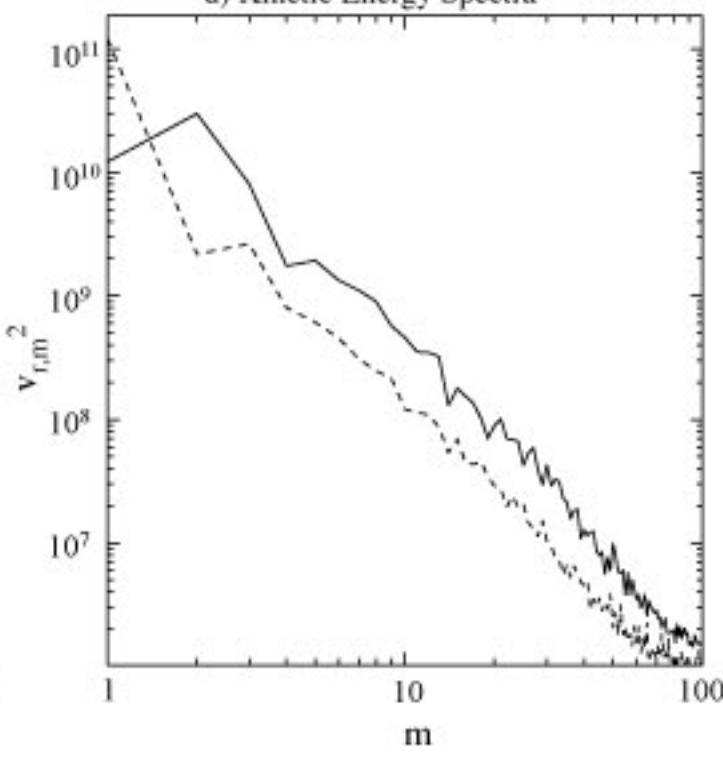


Figure 3: Low Rotation Rate